

See discussions, stats, and author profiles for this publication at: <https://www.researchgate.net/publication/231631011>

A Computational Study of Aluminum Hydroxide Solvation

ARTICLE *in* THE JOURNAL OF PHYSICAL CHEMISTRY A · OCTOBER 2001

Impact Factor: 2.69 · DOI: 10.1021/jp012171b

CITATIONS

35

READS

20

5 AUTHORS, INCLUDING:



Matti Hotokka

Åbo Akademi University

68 PUBLICATIONS 916 CITATIONS

SEE PROFILE



Kari Laasonen

Aalto University

140 PUBLICATIONS 5,805 CITATIONS

SEE PROFILE

A Computational Study of Aluminum Hydroxide Solvation

Atte J. Sillanpää,[†] Juha T. Päivärinta,[‡] Matti J. Hotokka,[‡] Jarl B. Rosenholm,[‡] and Kari E. Laasonen^{*,†}

Department of Chemistry, University of Oulu, P.O. Box 3000, FIN-90401 Oulun, Yliopisto, Finland, and Department of Physical Chemistry, Åbo Akademi University, FIN-20500 Åbo, Finland

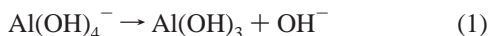
Received: June 6, 2001; In Final Form: September 4, 2001



We have modeled aluminum hydroxide solvation using static methods HF, DFT, and MP2 and different solvation models, as well as, Car–Parrinello molecular dynamics (CPMD). Two primary conformations were considered: $\text{Al}(\text{OH})_4^-$. The static methods predict generally similar structures and energies, but due to the difficult modeling of hydrogen bonds to the nearest solvation shells using the continuum methods, the geometries relative to the CPMD averages are quite different. Specifically, $\text{Al}(\text{OH})_4^-$ and $\text{Al}(\text{OH})_3 \cdot \text{H}_2\text{O}$ for $\text{Al}(\text{OH})_4^-$, the latter being slightly shorter and better defined, resulting in a total coordination number of 4. The $\text{Al}(\text{OH})_3 \cdot \text{H}_2\text{O}$, which are the strongest hydrogen bonds detected in the study. Also, in the CPMD simulations deprotonation/protonation events of these protons occurred, indicating the accessibility of both species at room temperature. The 3D environment of the hydroxy groups is $\text{Al}(\text{OH})_4^-$ and in general more like the solvation shell of H_2O than OH^- . Both vacuum and aqueous total spectra for the aluminum complexes are presented.

1. Introduction

Knowledge of the solvation of different ions in water is one of the key factors to understand reactions in solutions. Cation and proton hydration has been extensively studied, but explicit solvation studies of the hydroxy group are less frequent. We have studied the solvation structure and solution dynamics of aqueous aluminum hydroxide, which is an intermediate in the Bayer process where crystalline $\text{Al}(\text{OH})_3$ is extracted from bauxite in hot caustic solutions. There is both experimental^{1–3} and theoretical^{4–7} evidence that $\text{Al}(\text{OH})_4^-$ is the dominant species in caustic solution. Other monomeric and polymeric species have also been suggested to coexist. The fundamental reaction is therefore



Although the Bayer process has been used for a long time, the exact mechanism of the reaction is still unknown. The role of $\text{Al}(\text{OH})_4^-$ in the nucleation is also unknown. On the basis of semiempirical quantum chemical calculations, Gerson et al. suggested that the reaction might occur via minor species such as $\text{Al}(\text{OH})_3 \cdot \text{H}_2\text{O}$.⁵

It has also been claimed that the aqueous aluminate ion is monovalent and its coordination number, i.e., the number of ligands, is 4.⁸ It is quite clear that this kind of structure is strongly hydrated. If all solvent molecules in the first solvation shell were treated explicitly in theoretical calculations, the CPU time for the calculations would be large using any standard quantum chemical approaches (say Hartree–Fock or density functional theory). Different solvated aluminum species are of great interest to many research groups nowadays.^{2,4,6,7,9–12} Ruiz

et al. showed $\text{Al}(\text{OH})_4^-$ and $\text{Al}(\text{OH})_3 \cdot \text{H}_2\text{O}$. Tossel investigated various aluminum complexes using explicit water molecules on the first solvation shell and the Born solvation model for the bulk water.⁷ He found that the reaction



is clearly favored in the gas phase, but practically thermoneutral when solvation is taken into account using various approximations. His conclusion is, however, that when compared to the same analysis for the hydration of $\text{Al}(\text{OH})_2^{3+}$, for which experimental data are available, $\text{Al}(\text{OH})_4^-$. The use of continuum solvation models and static calculations may give unreliable structures and energies without the explicit description of the first solvation shell. To account for this, we report a comparison of the solvated aluminum structures as calculated by different static quantum chemical methods and Car–Parrinello molecular dynamics (CPMD) simulations where the outermost solvation shells are included. Lubin et al. have modeled cationic aluminum complexes using CPMD and the simulated annealing technique to study positively charged aluminum–water clusters.¹¹ However, as the Bayer process most likely involves negatively charged species due to the caustic environment and as Lubin et al. did not study dynamical phenomena, we have carried out a thorough investigation on the neutral aluminate system, which we anticipate to be the most important in the nucleation and surface integration processes.

2. Methods

We have investigated different hydrated $\text{Al}(\text{OH})_4^-$ (1) and $\text{Al}(\text{OH})_3 \cdot \text{H}_2\text{O}$ (2) structures and reaction 2 using Hartree–Fock (HF), density functional theory (DFT), and second-order

* E-mail: kari.laasonen@oulu.fi. Fax: +358-8-5331603.

[†] University of Oulu.

[‡] Åbo Akademi University.

perturbation theory (MP2). In the static DFT calculations we have used the BLYP and B3LYP hybrid functionals.^{13–16} In both the HF and DFT calculations we have also employed the polarized continuum model (PCM).^{17–21} The static calculations were performed using the 6-31+G** basis set^{22–25} with the Gaussian98 program,²⁶ and **1** and **2** for comparison also using the program Finger, see below.

The structures of the hydrated species were compared to those obtained from Car–Parrinello molecular dynamics simulations where the solvent is modeled explicitly. The Finger code (for CPMD and static plane wave calculations) has been developed at Helsinki University of Technology, Espoo, Finland. It is based largely on techniques presented at the paper by K. Laasonen et al.²⁷ We have used the BLYP density functional as it has been previously found to accurately reproduce the properties of water.^{28–30} The electron density has been described using a plane wave basis with a 25 Ry energy cutoff. To achieve the low cutoff, the wave function close to nuclei has been described using Vanderbilt-type pseudopotentials. The equations of motion were solved using the Verlet algorithm with a time step of 7.0 au (0.17 fs) and with a fictitious electron mass $\mu = 900$ amu. The microcanonical ensemble simulations were done in a cubic box with $a = 20.79$ bohr (11.0 Å) accommodating 41 water molecules and the $\text{Al}(\text{OH})_3$ moiety. CPU demand using 41 water molecules is close to the limit with our resources (one time step takes approximately 20 s using 64 CPUs on a Cray T3E supercomputer). A bigger periodic box would have further minimized the effect of the possible artifacts arising from the correlation of the outer solvent shells with their images. However, we feel that this is not a severe problem at least on the first solvation shell. Beyond 4 Å from aluminum the coordination number of water molecules is approximately constant and similar to bulk water. Further, a 3 ps CPMD simulation of $\text{Al}(\text{OH})_4^-$ in a 9.6 Å periodic cubic box with water molecules produced essentially identical RDFs and total spectrum.³¹

The following atomic masses for the nuclei were used: 2.0 amu for hydrogen, 16.0 amu for oxygen, and 27.0 amu for aluminum. We used deuterium instead of protium to increase the usable time step length as the experimental properties of heavy water are well-known and the chemistry will nevertheless be the same. For example, the total spectrum³¹ scaled with the reduced mass of the OH unit is practically indistinguishable from a H_2O (and a Li^+ ion) spectrum.³² Also, the radial distribution functions are very similar to experimental ones and those calculated for a larger system by Silvestrelli and Parrinello.³⁰ Despite the use of deuterium we will refer to it as H and hydrogen in this paper, except in the chapter where frequencies are discussed.

The first starting geometry was generated by placing a vacuum-optimized $\text{Al}(\text{OH})_3$ moiety in SPC water so that the overall density was 1123 kg m^{-3} (1018 kg m^{-3} for ^1H instead of ^2H). The coordinates were then optimized for 300 steepest-descent MD steps to relax the system's highest energy close contacts. Starting the CPMD dynamics from this configuration raised the temperature to approximately 200 K, after which it was adjusted to 300 K by slowly scaling the atomic velocities on successive time steps. This resulted immediately in water coordination to aluminum and a structure like **2**. Two subsequent simulations in solvent were performed. The starting configuration for the second simulation was generated as follows. The instantaneous coordinates of the first run at about 3 ps were modified so that other of the ligand water hydrogens was placed between two water molecules as far from aluminum as possible.


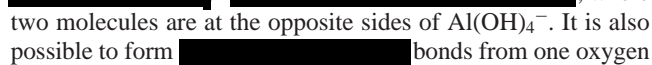
The system was then treated as before. The total simulation times were 11 and 9 ps, where data up to 3 and 1 ps, from the beginning, respectively, were removed from the analysis. The length of the vacuum CPMD simulation of **1** was 5 ps. Sufficient relaxation of the closest solvation shells is supported by the close similarity of the radial distribution functions (RDF) of **2** in the beginning of simulation 1 and end of simulation 2. From all the acquired data, especially the total spectrum³¹ and RDFs, we can conclude that water and hydroxy groups can be modeled using the BLYP functional and CP method.^{30,32,33} We note that in the absence of counterions the pH of the CPMD simulation is effectively 7.

3. Results

We have used the following notations to address the different O and H atoms in the computed structures: O^* and H^* refer to the oxygen and hydrogen atoms, respectively, which are directly bound to the aluminum ion forming the hydroxy groups. The ligand water molecule's atoms, i.e., the protonated hydroxy group, is depicted with O^\dagger and H^\dagger , respectively; see Figure 1.

3.1. Static Calculations. In all cases the HF-optimized Al–O distances are shorter than the B3LYP- and MP2-optimized ones (Table 1). The B3LYP bond distances are similar or at most 0.01 Å shorter than MP2-optimized ones. The use of the 6-31+G** basis set relative to the 6-31G* used by Ruiz et al. for the same complexes earlier⁶ does not alter the geometry of **1** but elongates the Al–O bonds slightly in **2**. We decided to use the 6-31+G** basis set. We consider this to describe the polarization effects properly and enable us to neglect corrections to the basis set superposition error (BSSE). The latter is effectively very small as the basis set is quite flexible and we are mainly interested in relative energies for which the BSSE is of similar size. The energies of the vacuum-optimized monomer structures with one to three explicit solvent molecules have been corrected for the zero point vibrational energy. An extra diffuse function on the hydrogen atoms would make the calculation substantially more demanding while the benefit is questionable. The charges derived from electrostatic potential (ESP) in aluminum and oxygen atoms of different species are quite similar in a vacuum with all methods (Table 2). The partial charges in $\text{Al}(\text{OH})_4^-$ aluminum and O^* atoms are 0.20–0.25 and 0.09–0.15 smaller, respectively, when compared to corresponding atoms in $\text{Al}(\text{OH})_3 \cdot \text{H}_2\text{O}$.

The effect of solvation was first studied by adding explicit water molecules to the naked structures. All methods predicted only one feasible conformation for $\text{Al}(\text{OH})_4^-$ with one explicit solvating water molecule. The water molecule forms two hydrogen bonds with the hydroxyl groups of $\text{Al}(\text{OH})_4^-$ (**3**). In the HF-optimized structures the intramolecular distances tend to be shorter and intermolecular distances longer than in B3LYP- and MP2-optimized structures. The hydrogen bond distances calculated by HF (2.07 Å) are about 0.1 Å longer than the B3LYP- (1.97 Å) and MP2-optimized (1.98 Å) ones. The stabilization energies for all hydrated $\text{Al}(\text{OH})_4^-$ complexes are listed in Table 3. These energies are the difference of the sum of noninteracting water molecules and the naked complex **1** compared to the complexes shown in Figure 1.

 where two molecules are at the opposite sides of $\text{Al}(\text{OH})_4^-$. It is also possible to form  bonds from one oxygen atom in $\text{Al}(\text{OH})_4^-$ (**5**). This was verified with all methods. B3LYP and MP2 produce also structures, where one of the water molecules forms a strong hydrogen bond and one van der Waals

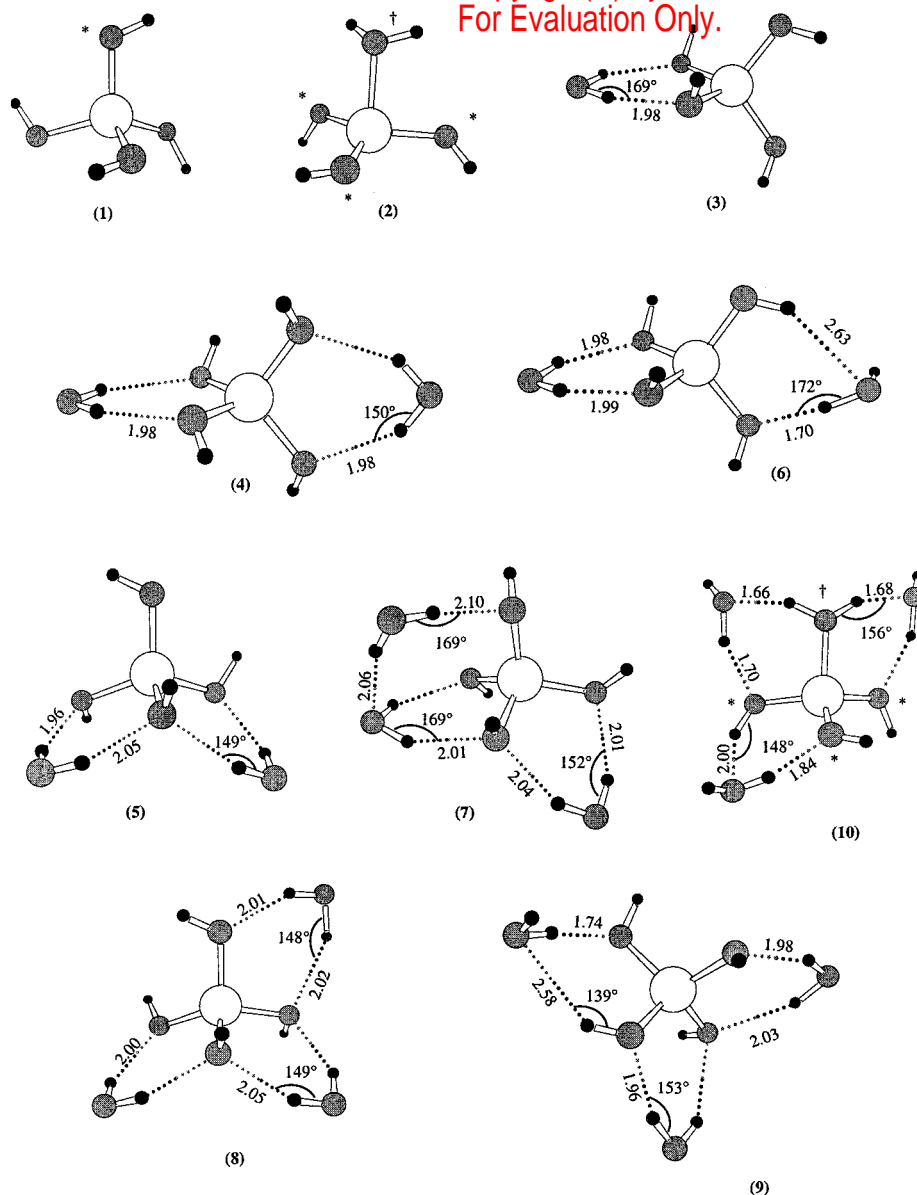


Figure 1. Characteristic vacuum minimum energy geometries (B3LYP). Bond lengths in angstroms and angles in degrees.

TABLE 1: Geometrical Parameters from Static Calculations and CPMD Simulations^a

property	HF		B3LYP		BLYP/6-31+G** vacuum	static vacuum	CPMD-Finger 41 waters	MP2 vacuum
	vacuum	PCM	vacuum	PCM				
Al(OH) ₄ ⁻								
Al—O*	1.77	1.76–1.77	1.79	1.79	1.81	1.80	1.80	1.80
O*—H*	0.94	0.95	0.96	0.96	0.97	1.00	1.00	0.96
Al(OH) ₃ •H ₂ O								
Al—O*	171–172	173	173–174	175	174–176	174–175	1.78	1.74–1.75
Al—O [†]	1.97	1.94	1.99	1.96	2.02	2.01	1.88	1.99
O*—H*	0.94	95	96	0.97	0.97	0.99	1.00–1.01	0.96
O [†] —H [†]	0.95	96	97	0.98	0.98	1.00	105–107	97
Al—O [†] H ₂ —plane ^b	124	161	116	157	115	118	~161 ^c	118

^a Aluminum–oxygen distances (Å) with different methods in the two primary structures. The static Finger results have been calculated as described in the computational details. CPMD results for **1** have been taken from the first 3.5 ps in the second simulation. Similarly, the CPMD results for **2** have been taken from time frames before 5.5 ps in the first simulation. Angles are given in degrees. ^b The blunt angle between the ligand water plane and the O[†]Al bond. ^c Average value given; the dynamic value fluctuates around 180°.

close contact with one hydroxy group (**6**). In this case the hydrogen bond distance was diminished to 1.70 and 1.73 Å as calculated with B3LYP and MP2, respectively. Water molecules forming two hydrogen bonds have distances of about 2.00–2.10 Å depending on the method. In the HF calculations each water molecule always formed two hydrogen bonds.

In the structures where a third water molecule was added to the solvation shell, we considered three possibilities. According to the B3LYP and MP2 calculations [redacted] = [redacted]. The HF method predicts highest

TABLE 2: ESP Charges of Atoms in the Naked Structures^a

structure	HF vacuum	HF PCM	B3LYP vacuum	B3LYP PCM	MP2 vacuum
Al(OH) ₄ ⁻					
Al	1.90	2.00	1.75	1.73	1.84
O*	-1.18	-1.27 to -1.28	-1.11	-1.17 to -1.18	-1.15
H*	0.45	0.52 to 0.53	0.42	0.49 to 0.50	0.44
Al(OH) ₃ •H ₂ O					
Al	1.65	1.71	1.45	1.52	1.60
O*	-1.06 to -1.09	-1.07 to -1.15	-0.96 to -0.99	-0.99 to -1.09	-1.02 to -1.07
O†	-0.78	-0.80	-0.70	-0.71	-0.77
H*	0.45 to 0.48	0.46 to 0.51	0.42 to 0.45	0.43 to 0.48	0.44 to 0.47
H†	0.48 to 0.49	0.50 to 0.51	0.45	0.46 to 0.48	0.48
Dimer					
Al	1.44 to 1.50	1.66 to 1.69	1.29 to 1.33	1.46 to 1.49	1.48 to 1.52
O _{free}	-0.99 to -1.01	-1.13 to -1.14	-0.90 to -0.91	-1.05 to -1.06	-0.98 to -0.99
O _{br}	-0.86	-0.92 to -0.93	-0.79	-0.78 to -0.80	-0.89
Trimer					
Al	1.51 to 1.58	1.66 to 1.74	1.31 to 1.45		1.52 to 1.65
O _{free}	-1.00 to -1.06	-1.10 to -1.17	-0.90 to -0.98		-0.97 to -1.05
O _{br}	-0.87 to -0.97	-0.94 to -1.06	-0.87 to -0.91		-0.91 to -1.00
Tetramer					
Al	1.53 to 1.66		1.39 to 1.65		
O _{free}	-1.02 to -1.13		-0.93 to -1.07		
O _{br}	-0.88 to -1.07		-0.81 to -1.06		

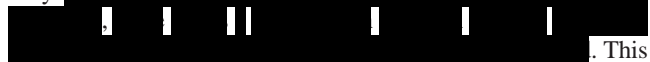
^a O* and H* denote the hydroxy group oxygens and hydrogens, respectively. O† and H† denote the ligand water atoms (see Figure 1); O_{free} and O_{br}, the free and bridging oxygen atoms in oligomeric structures, respectively.

TABLE 3: Stabilization by Complexation with Explicit Water Molecules^a

complex	no. of H ₂ O	method		
		HF	B3LYP	MP2
3	1	-54.2	-61.9	-65.1
4	2	-106.7	-121.5	-129.2
5	2	-102.4	-117.1	-125.4
6	2		-111.4	-117.9
7	3	-140.8	-164.1	-177.5
8	3	-143.0	-162.3	-175.8
9	3	-139.7	-161.5	-174.0

^a The stabilization energies of the different [Al(OH)₄]⁻•(H₂O)_n complexes (*n* = 1–3) calculated with different methods. Energies (kJ/mol) include zero point vibrational corrections.

stability to the structure where all three water molecules form two hydrogen bonds with Al(OH)₄⁻ (8). Also the structure where the third water molecule forms one hydrogen bond (9) and a weak donor bond was found to be a local minimum according to all methods. This illustrates the abundance of possibilities for solvent coordination. We conclude that when only

 This is illustrated, e.g., by the geometries 5 and 6, where either two long suboptimal hydrogen bonds are formed, or then one short, close to optimal hydrogen bond, and one vdW contact. This is an artifact of the solvation approximation, and we will show later that this chelating-type coordination on the first solvation shell is not relevant in dilute solutions (i.e., bulk water). Also, the RDFs of the CPMD simulations show that the hydrogen bonds are generally shorter than those found with only few explicit solvating waters. The partial charge of aluminum in Al(OH)₄⁻ is much more positive in the vacuum Hartree–Fock calculations relative to HF-PCM. Surprisingly, no difference was found in the B3LYP calculations.

Because there is quite good agreement between the B3LYP- and MP2-optimized geometries and energies for Al(OH)₄⁻, we have used only B3LYP in the evaluation of the explicitly

hydrated Al(OH)₃•H₂O structures. The most stable complex of Al(OH)₃•H₂O with one explicit solvent molecule has a stabilization energy of -65 kJ/mol. The solvent water forms hydrogen bonds with the hydroxyl group and the ligand water molecule. The second water molecule forms a similar hydrogen bond with a total stabilization energy of -114 kJ/mol. The most stable complex containing three explicit solvent molecules is according to the B3LYP calculation complex 10, as described in Figure 1 with a stabilization energy of -155 kJ/mol.

It is quite an enormous task to calculate all possible conformations of this system. As the energy differences between the conformations of Al(OH)₄⁻•(H₂O)₃ are quite small; below 5 kJ/mol, we report only some representative structures. There exists a large number of possible conformations when the next solvation shells are included in the calculations. Their optimization might also be deceptive because as we will show later, these clusters with only a few explicit water molecules produce geometries not found in the condensed phase. To study the complete first and second solvation shells, we have applied the Car–Parrinello molecular dynamics method.

The dimers, trimers, and tetramers investigated in this study are -(OH)₂Al(OH)₂Al(OH)₂-like neutral structures where each pair of aluminum atoms is bridged by two hydroxyl groups. These form also the main block in the gibbsite crystal. Harmonic frequencies were calculated for all the structures in a vacuum to ensure that the structure is a local minimum. The dimerization of Al(OH)₃•H₂O accompanied by the release of two water molecules has an energy change of -69, -58, and -55 kJ/mol, with HF, MP2, and B3LYP, respectively. The formation of the subsequent oligomers is also energetically favorable. At the MP2 level the CPU time needed to optimize the tetramer was prohibitively large. The beginning of the suggested crystallization reaction path with structures and energies is described in Figure 2.

The PCM model hardly changes the reaction energies and geometries for the formation of the dimers (Table 3) making them about 2 kJ/mol more favorable. This was expected because the computational solvation stabilization is pronounced only in reactions of small ions such as Al(OH)₄⁻. The bond distances

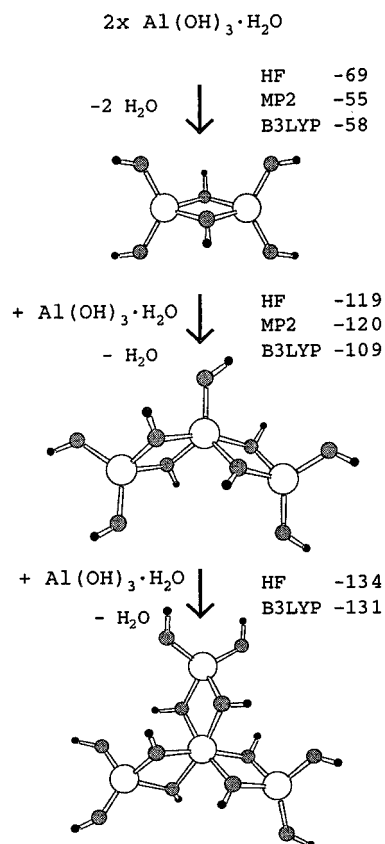


Figure 2. Structures and energies of the supposed nucleation reaction path optimized using HF (energies also for MP2 and B3LYP). Energies in kJ/mol.

increased about 0.02 Å and the aluminum–aluminum distances changed by 0.05–0.06 Å depending on the method.

3.2. Car–Parrinello Molecular Dynamics. The technical details of the simulations have been described in the Methods. We will concentrate on the following two simulations (although for $\text{Al}(\text{OH})_4^-$ we performed also one in a vacuum and one with 25 water molecules). In the first simulation the originally planar $\text{Al}(\text{OH})_3$ (vacuum structure) molecule was immersed in neutral water immediately capturing a water molecule forming the tetrahedral **2**; see Figure 1. This structure persisted for 5.5 ps, as can be seen in Figure 3. In the second a tetrahedral $\text{Al}(\text{OH})_4^-$ (**1**) and a H_3O^+ ion were placed in the periodic cell as far from each other as possible. The coordination environment and behavior of the system change when the proton attaches to the hydroxyl group and therefore the data from the above simulations have been split into two parts: set 1 for the configurations with four protons on the ligand shell thus corresponding to **1**, and set 2 for those configurations that correspond to $\text{Al}(\text{OH})_3 \cdot \text{H}_2\text{O}$ (**2**). The simulation data have been split also in other ways to evaluate certain properties. Specifically, the data prior to the protonation in simulation 2 have been used to characterize the anionic **1** geometry and frequencies, and data prior the deprotonation in simulation 1 for species **2**.

3.2.1. DYNAMICS: Proton Jumps, Diffusion. The oxygen atoms directly bound to aluminum were not observed to change with the free water molecules, and further, no configurations where five oxygen atoms were bound to aluminum were detected. The protons of the hydroxy groups, on the other hand, are less tightly bound and can be exchanged via the structure **2**.

In the first simulation the ligand water molecule remained attached to the Al ion for 5.5 ps, but after suitable second

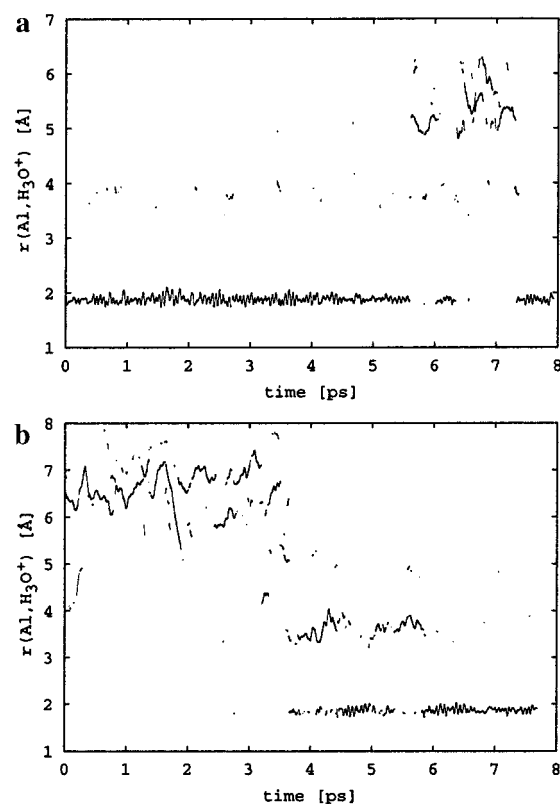


Figure 3. Proton diffusion in both simulations. The position of the excess proton (H_3O^+) has been taken as the oxygen atom bonded to three hydrogens (or a hydroxide ligand to two hydrogens: $\text{Al}-\text{OH}_2$). The distance between this oxygen and the aluminum atom has been plotted against the simulation time. Simulation 1 on the top and simulation 2 below. The dots at around 2 Å indicate structure **2** and thus demonstrate exchange between the two principal structures.

coordination sphere reorganization, the other proton transferred to a nearby water molecule. In Figure 3 it can be seen that several attempts for both of the ligand water protons to escape have failed during the first 5.5 ps, but then suddenly the proton has migrated to the second coordination shell via the first shell in less than 40 fs. The reversibility of the process is readily demonstrated at 6.3–6.6 ps. The mechanism of these jumps agrees with the one reported earlier for water.^{34–36} Namely, the water oxygen (or the hydroxy group if the transfer takes place to the aluminum moiety) first reduces its coordination number to three (Al^{3+} counts here as one) and then accepts the proton. The independence of this process of the starting geometry is supported by the data from the second simulation.

In the second simulation the proton, originally solvated with bulk waters, diffused through the simulation box according to the Grotthuss mechanism,³⁷ and finally protonated one of the hydroxy groups after 3.5 ps. The time scale of the jumps agrees qualitatively with the previously published data for protonated bulk water,³⁶ although quantitative values cannot be given due to the short simulation times. The excess proton, i.e., hydronium ion, has been identified as the oxygen atom, which has three protons within 1.32 Å, or that hydroxy oxygen atom which has two protons within the same range. In Figure 3 the distance between aluminum and these water oxygen atoms has been presented as a function of simulation time to describe the proton diffusion. Note that the Zundel ion or H_5O_2^+ produces a dot for both oxygen atoms in this representation.

Several protonation/deprotonation events for the aluminate ion were observed but the water molecule mediating the jump at the first solvation shell did not diffuse further and eventually

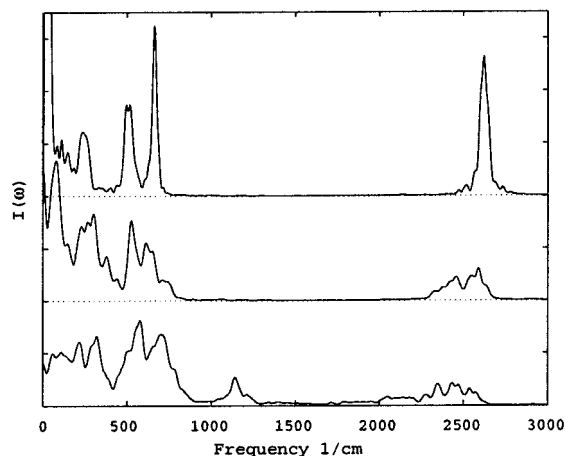


Figure 4. Total spectra obtained using Fourier transformation of the velocity autocorrelation function from the CPMD trajectories. From the top: Al(OD)_4^- (vacuum), Al(OD)_4^- (aq), and $\text{Al(OD)}_3 \cdot \text{D}_2\text{O}$ (aq).

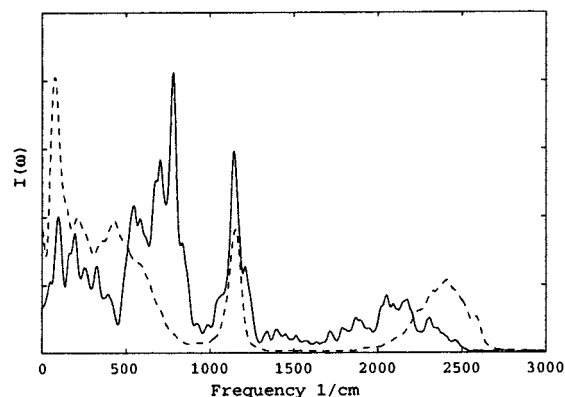


Figure 5. Total spectra as obtained using Fourier transformation of the velocity autocorrelation function. Bulk D_2O (dashed line) and ligand water (D_2O^+ , see Figure 1, solid line).

the same proton was transferred back to the aluminum hydroxy group again. In Figure 3 the proton can be seen to reside either on the OH ligand ($r \approx 1.9$ Å), on the first solvation shell ($r \approx 3$ –4 Å), or beyond the first solvation shell ($r > 5$ Å).

The time scale for AlOH donor and acceptor bonds as determined by the distance constraint ($r < 2.5$ Å) is qualitatively similar to bulk water. Both long-lived (entire simulation) and short-lived hydrogen bonds could be detected both in the acceptor and donor types, the typical lifetime being more than 1 ps. The donor hydrogen bonds from H^+ were present all the time.

It is difficult to compare the frequencies obtained with different methods directly, but we present the total spectra of **1** and **2** in Figure 4, as calculated in a realistic solvation environment, and discuss their relation to the spectra obtained with CPMD in a vacuum, static methods, and experiment. As our spectra are derived using the Fourier transform of the velocity autocorrelation function and it therefore gives no information of the IR or Raman absorption intensities, we will only compare the transition frequencies.

The ligand water deuterium atoms (D^+) span a large stretching frequency band (see Figures 4 and 5). The broadening of the stretching band to lower frequencies is due to the strong hydrogen bonding. Interestingly, the bending mode of the ligand water has shifted only little relative to bulk water. These frequencies are 1170 and 1160 cm^{-1} (BLYP), respectively, although this small difference is within the statistical error. It is therefore very difficult to distinguish between these species

on the basis of the ligand water bending mode, as it is obscured by the bulk water peak. The (Pearson) correlation between the O^+, O_w and D^+, O_w bond lengths (subscript w denoting the two first solvation shell water oxygen atoms), respectively, is negative (although small: -0.16 and -0.20), suggesting that the strong donor hydrogen bonds formed by the ligand water have a tendency to alternate. The B3LYP/PCM calculations yield generally similar results. The D_2O^+ bending in solution is at 1155 and 1150 cm^{-1} for a water molecule.

The O^*D^* stretching band in **1** has experienced a clear red shift relative to the CPMD vacuum spectrum but is generally similar to bulk water. In the neutral species **2** the band has spread even down to 2000 cm^{-1} , which is due to the stronger D^*-O_w donor hydrogen bonding in the absence of negative charge in the complex. On the other hand, as the static results do not produce proper donor hydrogen bonds to the hydroxy groups the lowest O^*D^* stretching frequencies derived from the explicit vacuum calculations are at 2820 and 2690 cm^{-1} , in structures **9** and **10**, respectively. The use of the PCM model reduces the vibrational frequencies more effectively, although still not to the same extent. The B3LYP/PCM frequencies in PCM-optimized geometries produce O^*D^* stretching bands at 2550–2600 and 2640–2660 cm^{-1} for **1** and **2**, respectively. Note that the order of these bands is different relative to the CPMD results, which we suggest to derive from the underestimated donor capability of the O^*D^* groups in **2** in the PCM calculations.

The only modes easily characterized from the CPMD data are the D_2O^+ bending and the OD stretchings. Many of the other modes have significant contributions of individual bendings and stretchings, but a qualitative assignment³⁸ gives some insight to the modes below 800 cm^{-1} . The symmetric Al– O^* stretching peaks of **1** are at 500–550 cm^{-1} both in a vacuum and in solution. The asymmetric stretching peak found in a vacuum at 650 cm^{-1} has shifted to 600 cm^{-1} in solution; simultaneously, the solvation broadens both peaks slightly. In **2** the Al– O^* symmetric stretching is only at a little higher frequency but broadened to 450–600 cm^{-1} . The asymmetric stretchings of **2** have two peaks at about 590 and 680 cm^{-1} due to the inequivalent oxygen atoms. A larger effect of solvation comes in the Al– O^*D^* bendings. In **1** at vacuum these are at 475–575 cm^{-1} , but in solution at 500–800 cm^{-1} , implying the coupling of this mode with the solvent. The Al– O^*D^* bendings are similar both in **1** and **2** and only the Al– O^+D^+ bendings are found at a little higher frequency. The O–Al–O bendings are found below 300 cm^{-1} . The B3LYP/PCM results predict the asymmetric stretchings for **1** and **2** at 690–730 and 795–810 cm^{-1} , respectively. The symmetric Al– O^* stretching mode for **1** is at 600, and for **2** it has split in two at 630 and 410 cm^{-1} , which have the major components in the Al– O^* and Al– O^+ bonds, respectively. As the highest frequency skeletal modes shift to lower frequency in the PCM calculations they shift to higher frequency in the CPMD case.

Agreement with experiment is not spectacular. The qualitatively identifiable symmetric Al–O stretching frequency from the CPMD simulations is about 100 cm^{-1} too low compared to experiment.³ The asymmetric Al–O bendings of **1**, which should be IR active, however, coincide with experiment and B3LYP/PCM results, while those of **2** are about 50 cm^{-1} too high. The experimentally predicted Al–OH bending peak at 950 cm^{-1} is missing in the B3LYP/PCM results but found with both CPMD and B3LYP/PCM at around 700 cm^{-1} , as predicted for AlOD.³ Comparison with more recent data is difficult due to our choice of deuterium, while most experiments use protium.^{3,4} The

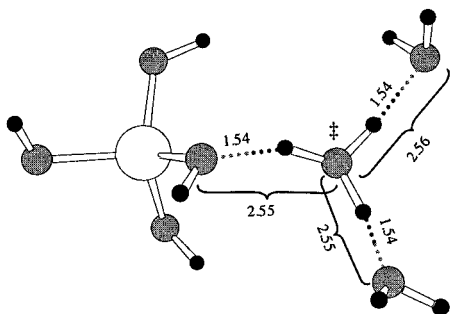


Figure 6. H_3O^+ hydronium ion on the first solvation shell of $\text{Al}(\text{OH})_4^-$, a snapshot from simulation 2.

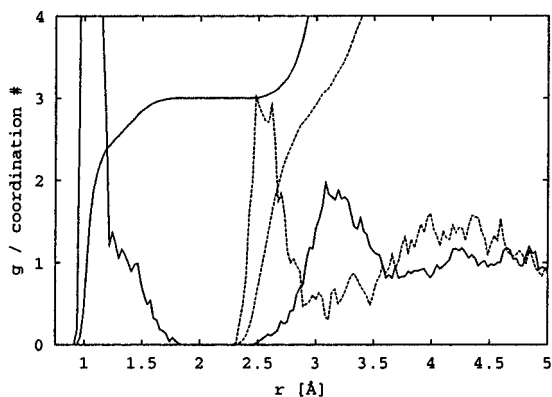


Figure 7. The RDFs and their integrals for the oxygen atom in the H_3O^+ ion (see Figure 6 for O^*), on the first solvation shell of $\text{Al}(\text{OH})_4^-$. $g(\text{O}^*,\text{H})$ solid line and $g(\text{O}^*,\text{O})$ dashed line, respectively.

isotope effect on different modes is complicated due to their coupling with solvent, and comparison with simple scaling fails.

The distinction between **1** and **2** might be made by the strong $\text{Al}-\text{O}^*$ stretching shoulder at 800 cm^{-1} . In **2** this extends to higher wavenumbers and appears in the frequency window not obscured by bulk water (see Figure 5). This is supported also by the B3LYP/PCM results. We note, however, that the error in the predicted symmetric (experimentally strongly polarized) $\text{Al}-\text{O}$ stretching frequency decreases the reliability of the calculated absolute frequencies, but they perhaps still offer valuable information of the relative frequencies and trends in shifts upon solvation. The lower frequency differences suffer from overlapping bulk water absorption and are less reliable due to the limited time scales of our simulations.

3.2.2. Structure. The analysis of the simulations in the following chapters is divided into sections, first considering briefly the hydronium ion, the solvation of the individual hydroxy groups, and finally the whole aluminum hydroxide.

3.2.2.1. Hydronium Ion. Previously, the proton has been shown to exist in water as two different hydronium ions: H_5O_2^+ and H_3O^+ .^{35–37,39} Both forms could be identified also in our simulations. In simulation 1, at around 6.1 and 6.5 ps, when the proton is close to an oxygen atom on the second solvation shell, it can be described as both hydronium ion forms, in succession. This can be seen in Figure 3, where the oxygen atom accommodating three protons is rapidly changing. H_3O^+ configuration can be also seen in the $g(\text{O}^*,\text{O})$ and $g(\text{O}^*,\text{H})$ (where the oxygen O^* on the first solvation shell primarily accommodating the proton has been used; see Figure 6), there are three hydrogens and oxygens inside the first RDF minima, which have also shifted to shorter distances (simulation 2 between 3.5 and 6.0 ps, Figure 7). The configuration is not completely symmetric, as the central oxygen is on average closer to the hydroxy group oxygen than the water oxygen.

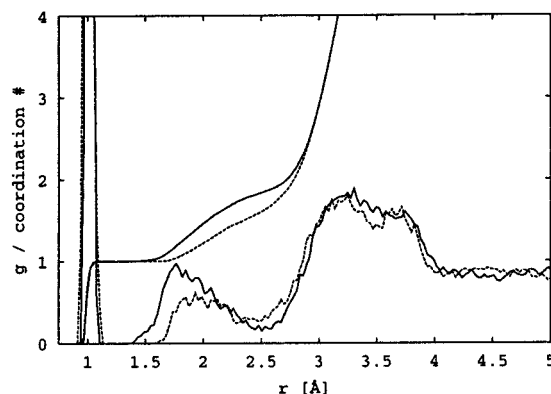


Figure 8. Stronger donor hydrogen bonds in the neutral complex, as illustrated by the RDFs and their integrals. $g(\text{H}^*,\text{O})$ for the neutral (solid line) and anionic (dashed line) complexes, respectively.

The configurations where the proton is midway between the hydroxy group and first shell water were only transitive and took place during the proton jumps. The dominant configurations are either as H_3O^+ on the first solvation shell or then as **2**, where the ligand water forms very strong hydrogen bonds. It might therefore be appropriate to describe the equilibrated system as a contact ion pair where there is one proton hopping between the one strongly hydrogen bound water molecule and the ligand water. The proportions of the two intermediates should be strongly influenced by pH as **1** is also relatively long-lived and in caustic solution would very likely dominate.

One has to be careful with the interpretation of the proton jumps and average geometries. As our simulations use classical nuclei, the proton position with respect to the closest oxygen atoms might favor the unsymmetrical (two minima) configurations relative to the symmetrical ones. Previously, the effect of the quantum description of the nuclei has been shown to prefer symmetric single minimum geometries for both OH^- and H^+ in water.³⁵

3.2.2.2. Hydroxy Group. The OH distances in the different hydroxy groups have been summarized in Table 1, together with the static values. The hydroxy OH bond distances are slightly shorter and the distribution more skewed at the long end than in bulk water. We shall now consider the OH solvation using the RDFs of each atom type. We find the hydrogen bonds in bulk water at $1.4\text{--}2.4\text{ Å}$, maximum at 1.8 Å (equal to the experimental value⁴⁰). The acceptor bonds in both configurations, i.e., **1** and **2**, appear at this same range. The total charge therefore does not affect the acceptor-type hydrogen bonding. However, the donor bonds exhibit a difference in the two structures: the peak at $g(\text{H}^*,\text{O})$ of **1** is at a larger distance than that of (**2**), see Figure 8. This can be rationalized by the negative charge reducing the donor capability. The integrated $g(\text{H}^*,\text{O})$ of both configurations converge at $r = 2.9\text{ Å}$, which means that if the coordination number is calculated at $r < 2.5\text{ Å}$, the negatively charged complex has fewer donor bonds.

$g(\text{O}^*,\text{O})$ and $g(\text{O}^*,\text{H})$ RDFs also reveal two different waters on the first solvation shell: water O's coordinated to H^+ are in the $2.3\text{--}2.75\text{ Å}$ range, maximum at 2.6 Å , and the water O's coordinated to O^*H^* hydroxy groups are in $2.5\text{--}3.25\text{ Å}$ range, illustrating again the stronger bonding of the ligand water to the first solvation shell; see Figure 9. The bulk water $g(\text{O},\text{O})$ RDF peak is at $2.5\text{--}3.2\text{ Å}$. The internal OH distances (i.e., $g(\text{O}^*,\text{H}^*)$, etc.), which are identical in the different configurations, also fall in the latter range. At these distances several different combinations are already possible. The fine structure in the $2.5\text{--}4.1\text{ Å}$ region comes from the superposition of the

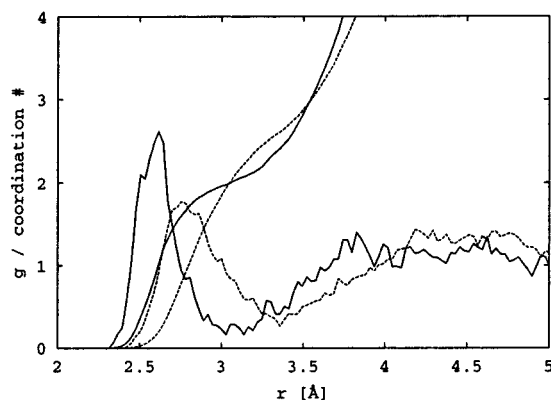


Figure 9. Stronger donor hydrogen bond of the ligand water, as illustrated by the RDFs and their integrals. $g(\text{O}^*,\text{O}_w)$ (dashed line) and $g(\text{O}^\dagger,\text{O}_w)$ (solid line) to solvent water oxygen atoms in $\text{Al}(\text{OH})_3\cdot\text{H}_2\text{O}$. O_w designate water oxygen atoms. See Figure 1 for O^\dagger and O^* .

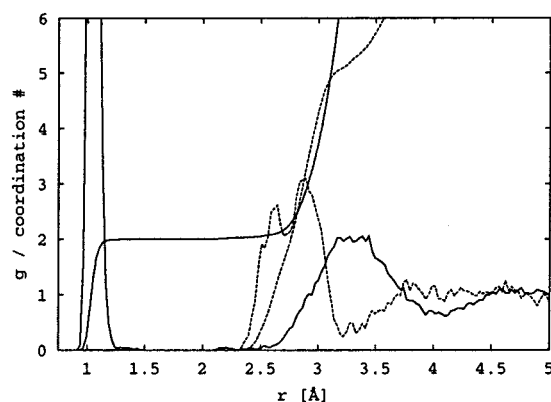


Figure 10. Fine structure in the ligand water coordination, as illustrated by the oxygen RDFs. The solid line is for $g(\text{O}^\dagger,\text{H})$ and its integral and the dashed line for $g(\text{O}^\dagger,\text{O})$ in $\text{Al}(\text{OH})_3\cdot\text{H}_2\text{O}$. The O^* , i.e., the mutual distances of oxygens bound to aluminum, appear in $g(\text{O}^\dagger,\text{O})$ at a range of 2.6–3.2 Å; compare with Figure 9.

hydroxy groups' internal distances and the first solvation shell waters. Specifically, the peak at 2.6–3.2 is from $g(\text{O}^\dagger,\text{O}^*)$, as seen in Figures 9 and 10. The internal peaks in $g(\text{O},\text{H})$ appear at 3.5–4.1 Å.

Total coordination numbers on the first solvation shell were evaluated using two methods to account for the different type of contacts. First, the number of water H atoms corresponding to the second maximum (1.24–2.5 Å) in the $g(\text{O}^*,\text{H})$ RDF (* means that both O^\dagger and O^* oxygens have been considered) was integrated to give the closest water H atoms. Similarly, the second maximum of $g(\text{H}^*,\text{O})$ (shown in Figure 11) was integrated to determine the closest water O atoms. The more strict method to determine the water molecules that were actually hydrogen bond were analyzed by restricting the angle of the hydrogen bond to more than 150° in addition to the distance limit. The geometry of the hydrogen bonds was also examined by plotting the bond distance vs the bond angle. See Figures 12 and 13.

In all data sets the first hydration shell consists of mainly donor and acceptor hydrogen-bonded water molecules (See Table 4). In addition, there are also water molecules within the second minimum of the $g(\text{O}^*,\text{H})$ pair correlation function that do not fulfill the hydrogen bond angle definition ($\varphi > 150^\circ$, for the $\text{H}\cdots\text{OH}$ bond). These are considered as van der Waals close contacts. They contribute about 0.4 per OH group and 0.2 for the ligand water adding up to 1.4 for the total coordination number in all sets. These close contacts are typically short-lived as compared to the actual hydrogen bonds.

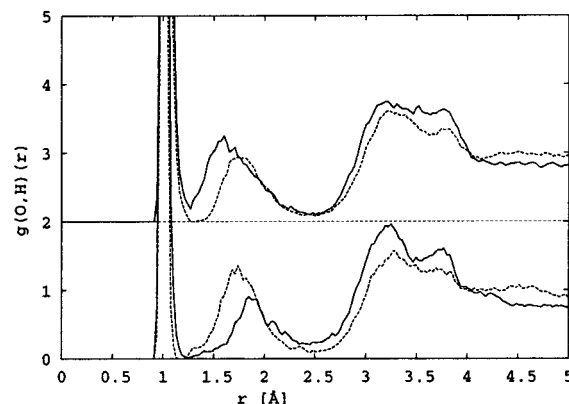


Figure 11. Difference in the total solvation structure between the neutral and anionic structures. $g(\text{H}^*,\text{O})$ (solid) and $g(\text{O}^\dagger,\text{H})$ (dashed) RDFs, set 1 (bottom) and set 2 (top). Superscripts * mean that both types of oxygen and hydrogen atoms have been included; see Figure 1 for definition. The peak at 3.5–4.1 Å is due to the mutual correlation of the H and O atoms in the hydroxy groups, i.e., $g(\text{O}^*,\text{H}^*)$.

The numbers of the acceptor and donor hydrogen bonds per OH group are roughly 1.5 and 0.6, respectively. However, if we look at the start of the second simulation, where the proton was not in the first solvation shell (or part of the ligand water), the donor bonds were slightly weaker and amounted only to 0.5 per OH group on average. This agrees with the result of Gale et al., who stated that the hydroxy groups preferably do not function as donors.⁴ Their complete first hydration shell consisted of four water molecules (relative to our 7–12), each forming a bridge between two hydroxy groups (6 atom ring) with acceptor and donor bond lengths of 1.69 and 2.06 Å, respectively. The difference in these results is due to the small number of explicit water molecules resulting in suboptimal individual hydrogen bonds.

The ligand water deserves some further characterization. Species 2 has two different types of oxygen and hydrogen atoms; the three equivalent OH groups and the ligand water. The looser binding of the latter protons can be clearly seen in all data (see, e.g., the spectra and RDFs), which reflect their higher acidity. It is also obvious from these data that the strongest hydrogen bonds are in the ligand water molecule, making it the natural place for deprotonation.

Comparison of the second peak of the bulk water, $g(\text{O}^*,\text{H})$, and $g(\text{H}^*,\text{O})$ RDFs reveal that the hydrogen bonds to the hydroxy groups are very similar to those in water. However, the former are not symmetric. The distribution of the hydrogen bond angle against H bond length (Figure 12) reveals the more strict geometry of the acceptor bonds relative to the donor bonds.⁴¹

The solvation of the hydroxy groups of aluminum hydroxide closely resembles the solvation of bulk water. The 3D coordination environment is approximately tetrahedral on average, like in the case of bulk water, as shown in Figure 13. Therefore the Al^{3+} ion can be regarded as a hydrogen atom common for each hydroxy group and it does not dramatically alter the first shell solvation structure. The differences in the RDFs at the third maximum of the hydroxy groups derive from hydroxy groups' correlation between themselves, which is naturally different relative to bulk water.

One major difference between the vacuum and solvated structures is the angle between the ligand water plane relative to the $\text{Al}-\text{O}^\dagger$ bond. In a vacuum the angle is between 115° and 120° with all methods. Adding two explicit solvating water molecules to the ligand water increases the angle to 136° .

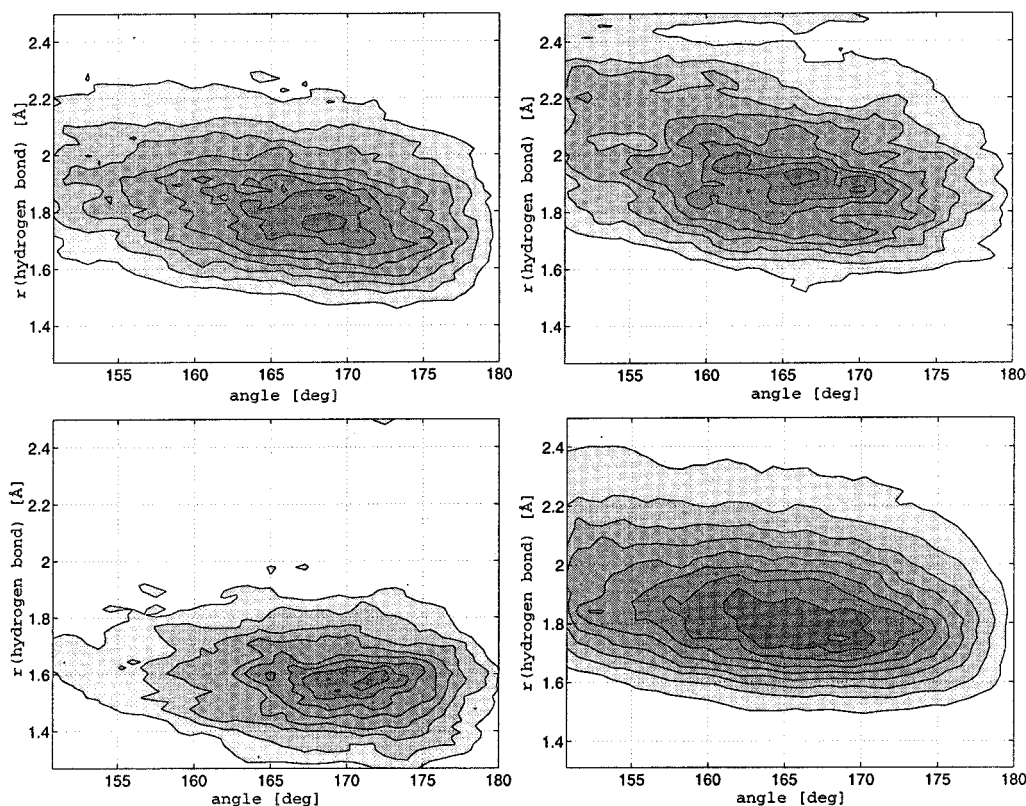


Figure 12. Spatial geometry of the hydrogen bonds as defined by the length of the hydrogen bond plotted against the $\text{O}^{\dagger}\text{H}^{\dagger}\cdots\text{O}_{\text{water}}$ or $\text{H}^{\dagger}\cdots\text{O}_{\text{water}}\text{H}_{\text{water}}$ blunt angles. Top left: O^* acceptor bonds. Top right: H^* donor bonds. Bottom left: H^{\dagger} donor bonds. Bottom right: bulk water (32 water molecule CPMD simulation). The isocontour spacing is linear.

However, as the waters simultaneously hydrogen bond to the O^*H^* groups, the resulting geometry is distorted with respect to the CPMD snapshots and averages. The CPMD average for this angle is 160° in accord with the PCM results. As the ligand water does not function as an acceptor, it has no need to coordinate in tetrahedral fashion. It can bond in a 180° angle, around which the plane is actually oscillating, to optimize its donor hydrogen bonds.

The planar coordination has no effect on the ligand water ESP charges. Also, the approximately 120° $\text{Al}-\text{O}^*\text{H}^*$ angles and sp^2 hybridization of both the O^* and O^{\dagger} atoms suggest that the bonding of the different oxygen atoms is basically similar. The longer $\text{Al}-\text{O}^{\dagger}$ distance can be explained by the smaller negative charge on O^{\dagger} . Therefore, we argue, that the planarity of the ligand water in the CPMD simulations is due to the more favorable donor hydrogen bonding.

3.2.2.3. Aluminum Hydroxide Moiety. The first solvation shell structure, divided into different bond types, in partitioned dynamics simulation sets has been collected in Table 4. First, we can see that irrespective of the division into the data sets according to the protonation state, the total number of hydrogen bonds formed by the ligands is 8.2–8.3, and if augmented with the other close contacts, 9.7–9.8. However, considering only the structure **1** when the proton is not nearby, i.e., the beginning of the second simulation, those numbers are about 0.5 smaller. According to the RDFs the hydrogen bonds are not shorter nor otherwise more localized to compensate their number. This might be a relaxation effect or else simply due to the importance of the donor bonds, which we found weaker in this case.

The $g(\text{Al},\text{O})$ and $g(\text{Al},\text{H})$ radial distribution functions (not shown) have some structure until $r = 5.5$ Å. However, if one plots the integrated $g(\text{H},\text{O})$ [1.25, 2.5 Å] as a function of the $r(\text{Al},\text{O})$ and $r(\text{Al},\text{H})$ to examine the hydrogen bonds in water,

one finds the following: The former becomes smooth after $r = 3.5$ Å and the latter after $r = 2.5$ Å, indicating that considering the solvation of the surrounding water it is relatively unperturbed after these distances.

The total H-bonded coordination numbers are primarily between 7 and 11. The bridging water molecules between two hydroxy groups seen in the static calculations count as two in this definition. These were very scarce being present approximately 1% of the time. Full hydration, i.e., a total hydrogen-bonded coordination number of 12 (see a snapshot Figure 14) was a rare event and present only for a few short periods.

An alternate way to determine the total coordination number would be to count the water molecules corresponding to the second maximum of $g(\text{Al},\text{O})$ (2.90–4.62 Å). After the ligand oxygens are subtracted, the resulting number (10.9) corresponds to three waters for each hydroxy group and two for the ligand water. However, we prefer the more detailed analysis explained above, which differentiates between the bonding modes and is less sensitive to the integration cutoff. On the other hand this illustrates that the solvation geometry is tetrahedral but that the individual hydrogen bonds, i.e., OH distances, frequently exceed the limiting distance of 2.5 Å, thus decreasing the number of simultaneous hydrogen bonds.

The distance to the second maximum in $g(\text{O}^{\dagger},\text{H})$ is reversed for set 1 and set 2; see Figure 11. The O^*H^* hydrogen bonds hardly change in the two sets; the difference comes from the $\text{O}^{\dagger}\text{H}^{\dagger}$ group. The strong donor bonds are missing from set 1, which reduces the integral of $g(\text{H}^{\dagger},\text{O})$ and shifts the maximum of the second peak to a longer distance. Simultaneously, even if the maximum of $g(\text{O}^{\dagger},\text{H})$ does not shift, its integral is reduced in set 2 as the ligand water molecule is inefficient in acceptor bonding. The average number of acceptor bonds to

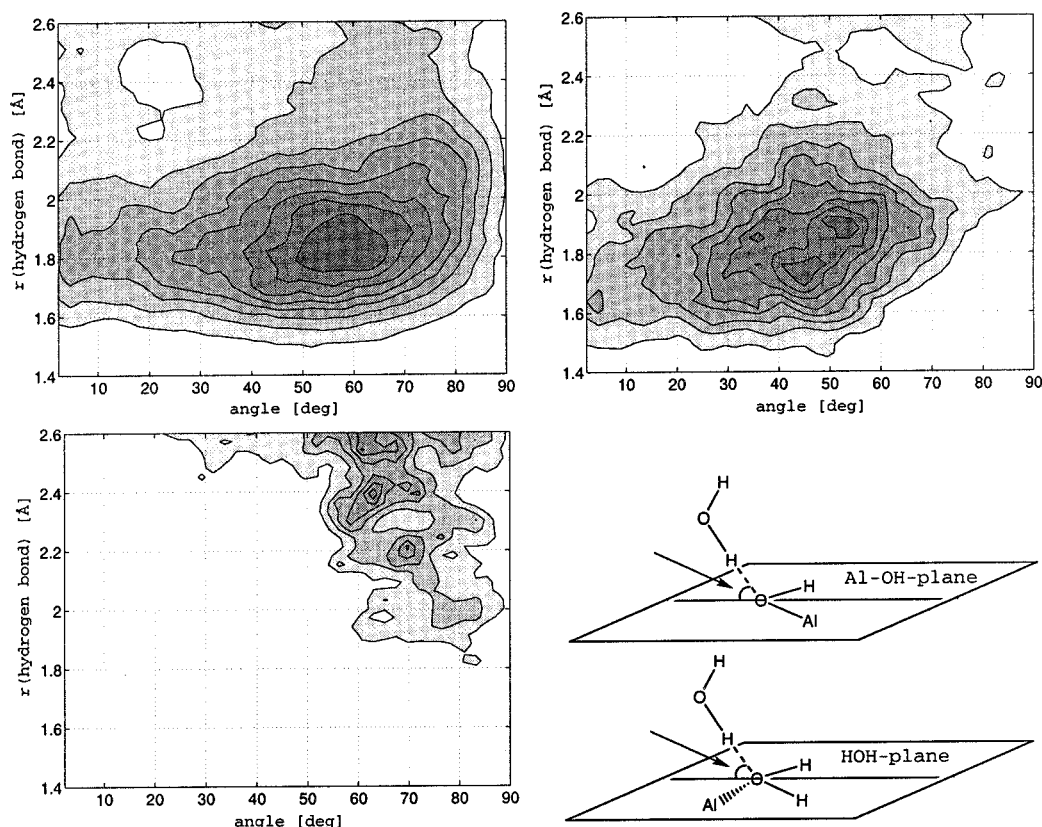


Figure 13. Illustration of the tetrahedral (water-like) coordination environment of the hydroxy groups. The distribution of the $r(\text{O}^\dagger \cdots \text{H}_{\text{water}})$ acceptor hydrogen bond length plotted against the acute angle between the Al–O*H* plane, HOH plane for bulk water, and H⁺O⁺H⁺ plane for the ligand water. Top left: bulk water. Top right: Al–O*H*. Bottom left: the ligand water. The isocontour spacing is linear. (Tetrahedral coordination appears at 55°).

TABLE 4: Coordination Numbers from CPMD Simulations^a

coordination type	set 1 ^b	set 2 ^b	all frames ^b	
	O* ^c	O* ^{†c}	O* ^{†c}	only O* ^{†s,c,d}
O _w within 2.5 Å from H* [†]	2.87	4.47	3.83	2.26
H within 1.25 Å from O* [†]	4	5	4.60	3
H within 2.5 Å from O* [†]	6.90	5.20	5.89	5.13
total acceptor bonds	6.03	4.35	5.03	4.39
total donor bonds	2.39	3.93	3.31	1.83
total coordination no.	9.77	9.68	9.72	7.39
total H-bonded coordination no.	8.42	8.28	8.34	6.22
acceptors per O* [†]	1.51	1.09	1.26	1.46
donors per O* [†]	0.60	0.98	0.83	0.61
total coordination no. per O* [†]	2.44	2.42	2.43	2.46

^a The average values are given. All (except the integers) have a Gaussian distribution with a mean deviation of 0.10–0.12. Hydrogen bond criteria have been given in the text. O*[†] means both types of ligand oxygen; see Figure 1. ^b Frame division. Depicts which instantaneous configurations have been used in the analysis. ^c Atoms whose coordination has been considered (includes also the corresponding hydrogen atoms). ^d Note that only three O*[†]s have been considered; scale with $4/3$ to compare with the other columns.

O[†] is only 0.08, and there are only 0.16 H's within 2.50 Å on average (excluding the H[†]'s; see also spatial arrangement in Figures 12 and 13.). This can be seen in the $g(\text{O}^\dagger, \text{H})$; where the second minimum is completely absent; see Figure 15. For the sake of argument if we consider the aluminum ion as a hydrogen atom common to all OH ligands, we can think of it as occupying both of the hydrogen bond acceptor sites for the ligand water. In set 1 the whole acceptor peak is at a closer distance. The amount of donor bonds is the largest in set 2 as it has five hydrogens on the ligands (3 times OH + H₂O).

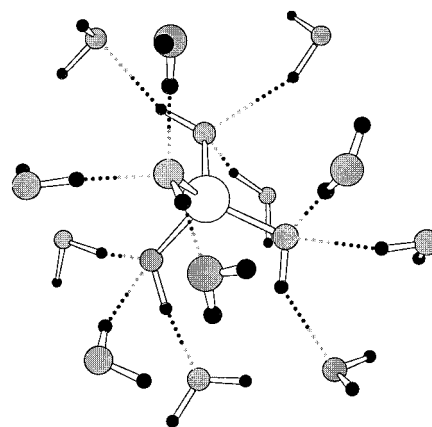


Figure 14. Full hydration, i.e., 12-coordination of the $\text{Al}(\text{OH})_4^-$ ion. A snapshot from simulation 2.

4. Discussion

The two different starting conformations used in the CPMD simulations evolved into the same general state. The immediate vicinity (i.e., ligands and the first solvation shell to a first approximation) is expected to relax quite quickly, but as the evolution of **2** momentarily to **1** after 5.5 ps shows, the reorganization at the second solvation shell to support proton transfer has significant impact on the aluminum itself. However, the information produced by the dynamical simulations revealed that actually neither of the two starting conformations clearly dominate, with perhaps some preference for **2**, but that their energies are such that they are both easily accessed already at room temperature. Also, as our dynamical simulation tends to maximize entropy, we argue that the proportions of the different

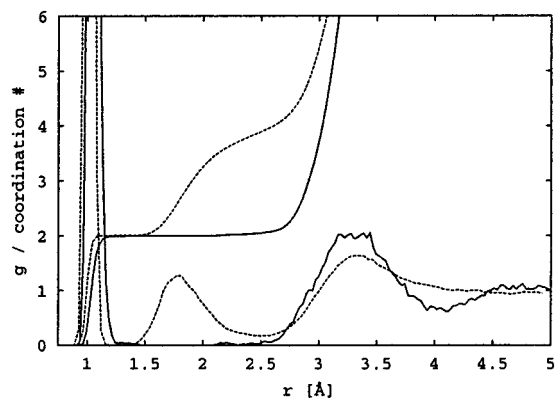


Figure 15. Illustration of the missing second peak of the ligand water RDF. The solid line is for $g(\text{O}^*,\text{H})$ and its integral and dashed line for $g(\text{O},\text{H})$ of bulk water (taken from a CPMD simulation with 32 water molecules).

configurations of the aluminate ion reflect their true occupation according to their free energies. The limited lengths of the simulations still allow only a rough estimate. Using static methods, the comparison is difficult due to the differences in modeling of the solvated proton. CPMD simulation is a straightforward solution to this inconsistency and simultaneously produces information of the dynamical behavior of the system. The relative stability as determined by the B3LYP/PCM calculations and experimental hydration free energy, -1105 kJ/mol (for protium, 298 K),⁴² prefers $\text{Al}(\text{OH})_3 \cdot \text{H}_2\text{O}(\text{aq})$ by 26 kJ/mol .⁴³ This agrees qualitatively with the CPMD results.

The static structures, calculated by the HF theory, deviate from the structures calculated by methods where correlation energy is taken into account, the former giving too short bonds. The BLYP functional, on the other hand, gives longer bonds than B3LYP and MP2. Also, the frequencies calculated using B3LYP are a little higher relative to those obtained with BLYP. The geometrical parameters obtained with the dynamical results based on the BLYP functional should be considered bearing this in mind. However, the Car–Parrinello molecular dynamics simulation results for the hydrated $\text{Al}(\text{OH})_4^-$ and $\text{Al}(\text{OH})_3 \cdot \text{H}_2\text{O}$ are quite different from the structures predicted by static quantum chemical calculations. In the CPMD simulations water molecules forming only a single hydrogen bond clearly dominate while in static calculations double hydrogen bonds are calculated to be more favorable. This is due to the small number of solvating water molecules used in the static calculations. Therefore, at least the complete first solvation shell is needed in order to realistically describe the solvation geometries, and possibly energies, and ultimately the Bayer reaction process. Optimizations with such clusters will be difficult due to the large amount of shallow potential minima.

The effect of solvation on the $\text{Al}-\text{O}^\dagger$ is also interesting: compare the values in Table 1. It can be seen that the PCM model correctly shortens the bond, but not to the extent that is seen in the CPMD averages. Also, the shortening of the $\text{Al}-\text{O}^\dagger$ bond is only 0.10 Å in the complexes where the ligand water has been coordinated to two solvating waters and an additional solvent molecule in various geometries. This clearly demonstrates the inadequate description of the solvation of the acidic H^\dagger protons. The water molecules on the second solvation shell are probably needed to sufficiently stabilize these protons.

The comparison of the coordination numbers of the ligand groups with bulk water is not straightforward. The aluminum ion reduces the coordination number as it does not form solvation bonds but is bonded to the ligands. However, if the

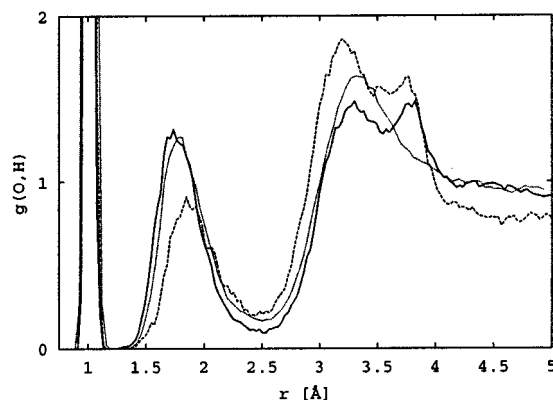


Figure 16. Illustration of the similarity of the acceptor H bond and bulk water H bonds. The RDFs are for $g(\text{H}^*,\text{O})$, $g(\text{O}^*,\text{H})$, and bulk water $g(\text{O},\text{H})$, drawn with dashed, solid, and dotted lines, respectively. The peak at $3.5\text{--}4.1 \text{ Å}$ is due to mutual hydroxy group correlation, i.e., $g(\text{O}^*,\text{H}^*)$.

hydroxy and ligand water groups' solvation is compared with that of half of a bulk water molecule, we will find that the ligand water has almost the same hydrogen bond and coordination numbers and that the hydroxy groups have smaller numbers. The structure of aqueous hydroxide ion has been reported to be tetrahedral (H_7O_4^-), with three acceptor bonds and one donor or square pyramidal (H_9O_4^-) with four acceptors and in maximum one donor.^{36,44,45} The donor bonds, however, are very weak. We find that this is not the case in the O^*H^* groups; see, e.g., their stretching frequencies and $g(\text{H}^*,\text{O})$. The average coordination of the O^*H^* groups thus resembles, also with the asymmetry of the hydrogen bonds considered, more bulk water than that of a hydroxide ion. See Figure 16.

In the end of both simulations the proton, i.e., the closest solvating water molecules forming the H_5O_2^+ or H_3O^+ ions are in contact with aluminum hydroxy groups. Due to the limited size of the simulation box this is not a surprise. This suggests that the preferred solvation structure would involve the proton very close to the anion. At least we can say, that there is no strong repulsion between individual solvation spheres of the hydronium ion and the anion. Instead, the solvation spheres overlap and the $\text{Al}-\text{OH}$ fragment takes the place of one solvating water molecule in the hydronium ion's solvation sphere. Deciding between the preference of **1** or **2** is, however, quite tentative due to the limited simulation times and simulation box size.

5. Conclusions

In the combined static and dynamic computational study we have shown that the energies of the anionic $\text{Al}(\text{OH})_4^-$ and neutral $\text{Al}(\text{OH})_3 \cdot \text{H}_2\text{O}$ are both accessible at room temperature. Both species form strong hydrogen bonds to the first solvation shell, which consists of eight to nine water molecules (and hydrogen bonds) on average. The acceptor hydrogen bonds are favored over the donor bonds by 1.5 to 0.6 per OH group, respectively, the former being almost identical to those in bulk water. The ligand water in the neutral complex contains two very acidic protons (deuteriums), which were observed to transfer to the solvent during CPMD simulations. The acidity is further supported by the bond lengths and total spectrum,³¹ where a wide band from 2600 to 1200 cm^{-1} is observed. Also, the total spectra of the aluminate ions are presented, where we find a possibly detectable difference at 800 cm^{-1} .

The static results utilizing HF, B3LYP, BLYP, and MP2 calculations and either explicit solvent molecules or the PCM

continuum model predict different geometries relative to the CPMD data. Due to the small number of explicit water molecules ($n < 4$), they formed chelates to maximize the number of hydrogen bonds. This results in suboptimal geometries that were not detected in the CPMD simulations and we classify them as gas-phase artifacts.

Acknowledgment. We express our gratitude for the (CSC) Center for Scientific Computing in Finland, The Magnus Ehnrooth's foundation, Tor, Joe and Pentti Borg's foundation, and the Academy of Finland for financial support (grant no. 40559). J.P. gratefully acknowledges the help of Maija Lahtela-Kakkonen of CSC for the help in the solvation model calculations.

References and Notes

- (1) van Straten, H. A.; Holtkamp, B. T. W.; de Bryun, P. L. *J. Colloid Interface Sci.* **1984**, *98*, 343–362.
- (2) Radnai, T.; May, P. M.; Hefter, G. T.; Sipos, P. *J. Phys. Chem. A* **1998**, *102*, 7841–7850.
- (3) Moolenaar, R. J.; Evans, J. C.; McKee, L. D. *J. Phys. Chem.* **1970**, *74*, 3629–3636.
- (4) Gale, J. D.; Rohl, A. L.; Watling, H. R.; Parkinson, G. M. *J. Phys. Chem. B* **1998**, *102*, 10372–10382.
- (5) Gerson, A. R.; Ralston, J.; Smart, R., St. C. *Colloids Surf.* **1996**, *110*, 105–117.
- (6) Ruiz, J. M.; McAdon, M. H.; Garcés, J. M. *J. Chem. Phys. B* **1997**, *101*, 1733–1744.
- (7) Tossel, J. A. *Am. Mineral.* **1999**, *84*, 1641–1649.
- (8) Glastonbury, J. R. *Chem. Ind.* **1969**.
- (9) Bakker, A.; Hermansson, K.; Lindgren, J.; Probst, M.; Bopp, P. A. *Int. J. Quantum Chem.* **1999**, *75*, 659.
- (10) Wasserman, E.; Rustad, J. R.; Xantheas, S. S. *J. Phys. Chem. B* **1997**, *106*, 1733.
- (11) Lubin, M. I.; Bylaska, E. J.; Weare, J. H. *Chem. Phys. Lett.* **2000**, *322*, 447–453.
- (12) Kubicki, J. D.; Sykes, D.; Apitz, S. E. *J. Phys. Chem. A* **1999**, *103*, 903–915.
- (13) Becke, A. D. *J. Chem. Phys.* **1993**, *98*, 5648–5652.
- (14) Becke, A. D. *Phys. Rev. A* **1988**, *38*, 3098.
- (15) Lee, C.; Yang, W.; Parr, R. G. *Phys. Rev. B* **1988**, *37*, 785.
- (16) Miechlich, B.; Savin, A.; Stoll, H.; Preuss, H. *Chem. Phys. Lett.* **1989**, *157*, 200.
- (17) Barone, V.; Cossi, M.; Tomasi, J. *J. Comput. Chem.* **1998**, *19*, 404.
- (18) Cancès, M. T.; Mennucci, V.; Tomasi, J. *J. Chem. Phys.* **1997**, *107*, 3032.
- (19) Cossi, M.; Barone, V.; Cammi, R.; Tomasi, J. *J. Chem. Phys. Lett.* **1996**, *255*, 327.
- (20) Miertus, S.; Scrocco, E.; Tomasi, J. *J. Chem. Phys.* **1981**, *55*, 117.
- (21) Miertus, S.; Tomasi, J. *Chem. Phys.* **1982**, *65*, 239.
- (22) Clark, T.; Chandrasekhar, J.; Schleyer, P. V. R. *J. Comput. Chem.* **1983**, *4*, 294.
- (23) Ditchfield, R.; Hehre, W. J.; Pople, J. A. *J. Chem. Phys.* **1971**, *54*, 724.
- (24) Hariharan, P. C.; Pople, J. A. *Theo. Chim. Acta* **1973**, *28*, 213.
- (25) Hehre, W. J.; Ditchfield, R.; Pople, J. A. *J. Chem. Phys.* **1972**, *56*, 2257.
- (26) Frisch, M. J.; Trucks, G. W.; Schlegel, H. B.; Scuseria, G. E.; Robb, M. A.; Cheeseman, J. R.; Zakrzewski, V. G.; Montgomery, J. A.; Stratmann, R. E.; Burant, J. C.; Dapprich, S.; Millam, J. M.; Daniels, A. D.; Kudin, K. N.; Strain, M. C.; Farkas, O.; Tomasi, J.; Barone, V.; Cossi, M.; Cammi,
- (27) Mennucci, B.; Pomelli, C.; Adamo, C.; Clifford, S.; Ochterski, J.; Petersson, G. A.; Ayala, P. Y.; Cui, Q.; Morokuma, K.; Malick, D. K.; Rabuck, A. D.; Raghavachari, K.; Foresman, J. B.; Cioslowski, J.; Ortiz, J. V.; Stefanov, B. B.; Liu, G.; Liashenko, A.; Piskorz, P.; Komaromi, I.; Gomperts, R.; Martin, R. L.; Fox, D. J.; Keith, T.; Al-Laham, M. A.; Peng, C. Y.; Nanayakkara, A.; Gonzalez, C.; Challacombe, M.; Gill, P. M. W.; Johnson, B. G.; Chen, W.; Wong, M. W.; Andres, J. L.; Head-Gordon, M.; Replogle, E. S.; and Pople, J. A. *Gaussian 98*, revision A.6 ed.; Gaussian Inc.: Pittsburgh, PA, 1998.
- (28) Laasonen, K.; Pasquarello, A.; Car, R.; Lee, C.; Vanderbilt, D. *Phys. Rev. B* **1993**, *47*, 10142–10153.
- (29) Sprik, M.; Hutter, J.; Parrinello, M. *J. Chem. Phys.* **1996**, *105*, 1142–1152.
- (30) Tassaing, T.; Bellissent-Funel, M.-C.; Zhao, H.; Beysens, D.; B. Guillot, B.; Guissani, Y. *J. Chem. Phys.* **1997**, *107*, 2942–2949.
- (31) Silvestrelli, P. L.; Parrinello, M. *J. Chem. Phys.* **1999**, *111*, 3572–3580.
- (32) Note. *The total spectrum means the Fourier transform of the velocity autocorrelation function of the coordinates of the atomic nuclei. The locations of the peaks correlate with the infrared and Raman spectra although no information on the spectroscopic intensities is acquired.*
- (33) Lyubartsev, A. P.; Laasonen, K.; Laaksonen, A. *J. Chem. Phys.* **2001**, *114*, 3120–3126.
- (34) Laasonen, K.; Sprik, M.; Parrinello, M. *J. Chem. Phys.* **1993**, *99*, 9080–9089.
- (35) Day, T. J. F.; Schmitt, U. W.; Voth, G. A. *J. Am. Chem. Soc.* **2000**, *122*, 12027–12028.
- (36) Tuckerman, M. E.; Ungar, P. J.; von Rosenvinge, T.; Klein, M. L. *J. Chem. Phys.* **1996**, *100*, 12878–12887.
- (37) Tuckerman, M.; Laasonen, K.; Sprik, M.; Parrinello, M. *J. Chem. Phys.* **1995**, *103*, 150–161.
- (38) Vuilleumier, R.; Borgis, D. *J. Chem. Phys.* **1999**, *111*, 4251–4266.
- (39) Note. *We analyzed the type of vibration by projecting the atomic motion onto, e.g., the Al–O bond, O–Al–O angle, etc. and compared the resulting intensity with the total spectrum obtained by Fourier transforming the velocity autocorrelation function over all atoms. This simple analysis reveals that several modes, especially at the low frequency end, are strongly coupled (stretching modes are not pure stretch, etc.), just as in the case of the static calculations (G98) employing the harmonic approximation. The analysis, however, localizes some modes and is therefore useful in assigning the spectrum. The symmetric and asymmetric Al–O stretching modes were assigned by Fourier transforming the sum of all bonds (symmetric) and all permutations of the bond velocities with 180° phase angle (asymmetric) as a function of simulation time.*
- (40) Sagnella, E. D.; Tuckerman, M. E. *J. Chem. Phys.* **1998**, *108*, 2073–2083.
- (41) Soper, A. K.; Bruni, F.; Ricci, M. A. *J. Chem. Phys.* **1997**, *106*, 247–254.
- (42) Note. *The plots have not been normalized with respect to the volume of the angle–distance element. Were it so, the probability density would be the highest with a linear hydrogen bond decreasing rapidly with decreasing angle.*
- (43) Tissandier, M. D.; Cowen, K. A.; Feng, W. Y.; Gundlach, E.; Cohen, M. H.; Earhart, A. D.; Coe, J. V.; Tuttle, T. R., Jr. *J. Phys. Chem. A* **1998**, *102*, 7787–7794.
- (44) Note. *Naked B3LYP/PCM-optimized structures' frequencies were calculated using finite differences, the harmonic approximation, and the PCM model. We also determined the same free energies using the vacuum geometries, frequencies, and single point PCM solvation free energies to examine the validity of their use instead of the strictly PCM data. This resulted in an energy difference of 48 kJ/mol. The same analysis prefers 10 to 9 + H⁺(aq) by 63 kJ/mol, which suggests that partial inclusion of the first solvation shell does not alter the order of preference.*
- (45) Masamura, M. *Chem. Phys. Lett.* **2001**, *339*, 279–289.
- (46) Tunon, I.; Rinaldi, D.; Ruiz-Lopez, M. F.; Rivail, J. L. *J. Phys. Chem.* **1995**, *99*, 3798–3805.